CARPATHIAN J. MATH.
Volume **42** (2026), No. 2,
Pages 267-286

Online version at https://www.carpathian.cunbm.utcluj.ro/
ISSN 1584-2851 (Print edition); ISSN 1843-4401 (Electronic)
DOI: https://doi.org/10.37193/CJM.2026.02.05

Classifying compressive strength of clay bricks using an inertial projected forward-backward algorithm

WATCHARAPORN CHOLAMJIAK[1], SIWAT LAWANWADEEKUL[2], KUNRADA KANKAM[3], PRASIT CHOLAMJIAK[1], AND NIPA JUN-ON[4]

ABSTRACT. The enduring popularity of clay bricks as a construction material can be attributed to their affordability. Nevertheless, the elevated temperatures necessary to attain the desired physical and mechanical characteristics result in substantial energy consumption and the emission of thermal pollutants. Accurately classifying clay bricks is essential in evaluating their suitability for construction purposes, with compressive strength being a critical parameter. The present study introduces new projected forward-backward algorithms for solving constrained convex minimization problems by using line search techniques to classify the compressive strength of clay bricks. The algorithm performs better than current methodologies, displaying exceptional precision, recall, F1 score, and accuracy.

As a numerical result, the finding highlight the significance of water absorption for classifying compressive strength. The bulk density is directly influenced by the size of additives, whereas the firing temperature, firing shrinkage, and apparent porosity exhibit interrelationships throughout the firing process. A comprehensive understanding of these parameters is pivotal in enhancing the clay brick manufacturing process and facilitates informed decision-making about material selection and structural design. Moreover, the algorithm can enhance machine learning methodologies in materials science and engineering applications.

1. INTRODUCTION

The affordability of clay bricks as a construction material has contributed to their enduring popularity over many centuries. To meet the desired physical-mechanical properties of clay bricks, the firing procedure necessitates high firing temperatures, which leads to significant energy consumption and thermal pollution [28, 15]. Since the phase transformation of clay at various temperatures directly impacts the final product's physical and mechanical characteristics [5, 16].

In civil and structural engineering, the compressive strength of clay bricks is a paramount property that dictates their suitability and safety for construction purposes. Moreover, precisely and effectively classifying the compressive strength is critical for ensuring quality control, selecting appropriate materials, and designing structures [31, 1, 17]. Traditionally, this critical property is determined through destructive laboratory testing, a process that is not only time-consuming and expensive but also results in the loss of material.

Consequently, there is a significant and practical need for reliable, non-destructive methods to classify brick strength based on easily measurable physical or visual parameters. This challenge motivates the development of robust computational models capable of learning the complex relationship between brick features and their mechanical properties.

Received: 26.04.2025. In revised form: 16.08.2025. Accepted: 18.11.2025
2020 *Mathematics Subject Classification.* 65K05, 90C25, 90C30, 90B30, 90B99.
Key words and phrases. *constrained convex minimization problem; machine learning; projected forward-backward algorithm; clay bricks; compressive strength; construction material classification.*
Corresponding author: Nipa Jun-on; nipa.676@g.lpru.ac.th

This classification task can be effectively modeled as a machine learning problem, which, in turn, can be formulated mathematically as a constrained convex minimization problem. Specifically, the goal is to find a set of model parameters that minimizes a loss function subject to certain constraints. This formulation allows us to leverage the powerful framework of proximal algorithms, which are designed to efficiently solve such composite optimization problems.

The projected forward-backward splitting algorithm is a fundamental and widely used method for solving this class of constrained convex minimization problems. However, its convergence rate can be slow, which presents a bottleneck in large-scale applications. To overcome this limitation, researchers have explored various acceleration strategies. One prominent approach is the inertial technique, which incorporates a momentum term from previous iterates to speed up convergence. Another avenue for improvement lies in modifying the iterative structure itself, with multi-step processes like the Ishikawa iteration [10] offering potential benefits in terms of stability and convergence behavior under certain conditions. Despite these advances, the synergy of combining inertial techniques with a multi-step iterative framework for projected splitting methods remains an area ripe for exploration.

Motivated by the need for a more efficient and robust algorithm for the brick classification problem, in this paper, we aim to design new projected forward-backward algorithms based on Ishikawa [10] iterations for solving the constrained convex minimization problems and provide weak convergence theorem for the proposed algorithm by using the inertial technique, to classify the compressive strength of clay bricks. We also show that the proposed algorithm outruns other methods in the literature. Moreover, the numerical results show that it efficiency in terms of precision, recall, F1 score and accuracy.

The subsequent sections of this paper are organized in the following manner: Section 2, as mathematical background section, delineates the methodology employed in this study, encompassing the theoretical underpinnings of the the inertial projected forward-backward algorithm. In section 3 of the paper, we construct our main theorem, while the experimental configuration, datasets, and metrics for performance evaluation are presented in section 4 of numerical experiments. The study is discussed in real-world application and concluded in section 5 and section 6 respectively, wherein the contributions of the research are emphasized.

2. Mathematical Background

The core objective of this research is to develop a reliable method for classifying the compressive strength of clay bricks from non-destructive features. From a computational standpoint, this is a supervised machine learning classification task. We aim to train a model that learns a mapping from a set of input features to a discrete class label.

The process of training such a model can be rigorously framed as a constrained convex minimization problem. This powerful mathematical structure is foundational to a vast array of modern machine learning algorithms. Many real-world problems in applied science and engineering, such as image and signal processing and machine learning [9, 11, 12, 14, 25, 26, 27], can be formulated in the form of a constrained convex minimization problem:

$$\min_{\phi\in\Omega}(\wp(\phi)+\Im(\phi)) \tag{2.1}$$

where Ω is a nonempty closed convex subset of a Hilbert space H and $\wp, \Im : H \to \mathbb{R}\cup\{+\infty\}$ are proper, convex and lower semicontinuous functions that $\wp$ is differentiable on

H. The goal is to find a set of model parameters in a Hilbert space that minimizes an objective function over a set of feasible parameters.

By Fermat's rule, we see that $\bar{\phi}$ is an optimal solution to (2.1) if and only if

$$\begin{aligned} \bar{\phi} \in \Omega \text{ and } 0 \in \beta\nabla\wp(\bar{\phi}) + \beta\partial\Im(\bar{\phi}) \quad &\Leftrightarrow \quad \bar{\phi} \in \Omega \text{ and } (I - \beta\nabla\wp)(\bar{\phi}) \in (I + \beta\partial\Im)(\bar{\phi}) \\ &\Leftrightarrow \quad \bar{\phi} \in \Omega \text{ and } \bar{\phi} = \text{prox}_{\beta\Im}(\bar{\phi} - \beta\nabla\wp(\bar{\phi})), \end{aligned} \tag{2.2}$$

where $\beta > 0$, $\text{prox}_{\beta\Im} = (I + \beta\partial\Im)^{-1}$ stands for the proximal operator of $\Im$, $\nabla\wp$ is the gradient of $\wp$ and $\partial\Im$ is the subdifferential of $\Im$. The subdifferential of $\Im$ is the set valued operator $\partial\Im : H \to 2^H$ which is defined by

$$\partial\Im(\phi) = \{\psi \in H | \Im(\varphi) - \Im(\phi) \geq \langle \psi, \varphi - \phi \rangle, \varphi \in H\}.$$

If $\Omega = H$, then (2.1) solves the unconstrained convex minimization problem:

$$\min_{\phi \in H}(\wp(\phi) + \Im(\phi)), \tag{2.3}$$

which is equivalent to the fixed point equation: $\phi = \text{prox}_{\beta\Im}(\phi - \beta\nabla\wp(\phi))$, where $\beta > 0$. For solving (2.3), we can construct a simple iteration: let $\phi^0 \in H$ and

$$\phi^{n+1} = \text{prox}_{\beta\Im}(\phi^n - \beta\nabla\wp(\phi^n)), \tag{2.4}$$

where $\beta > 0$. By this point of view, we know that (2.4) is called a classical forward-backward splitting algorithm (FBS). As a consequence, it has been studied by many authors (see [11, 12, 25, 4, 13]).

Let $\phi \in H$, we know that the orthogonal projection of ϕ onto a nonempty, closed and convex subset C of H is defined by

$$P_C\phi := \underset{\psi \in C}{\text{argmin}} \|\phi - \psi\|^2. \tag{2.5}$$

We know that

$$\|P_C\phi - \psi\|^2 \leq \|\phi - \psi\|^2 - \|P_C\phi - x\|^2,$$

for all $y \in C$. From (2.2) and (2.5), we can define a simple method for solving (2.1) as follows: let $\phi^0 \in H$ and

$$\phi^{n+1} = P_\Omega(\text{prox}_{\beta\Im}(\phi^n - \beta\nabla\wp(\phi^n))), \tag{2.6}$$

where $\beta > 0$. The method (2.6) is called a projected forward-backward splitting algorithm (PFBS).

In 2005, Combettes and Wajs [6] proposed the relaxed version of FBS (FBS-CW) which is generated by $\phi^0 \in H$, $\lambda_n \in [\varepsilon, 1]$ and

$$\phi^{n+1} = \phi^n + \lambda_n(\text{prox}_{\beta_n\Im}(\phi^n - \beta_n\nabla\wp(\phi^n)) - \phi^n), \tag{2.7}$$

where $\varepsilon \in (0, \min\{1, 1/L\})$, $\beta_n \in [\varepsilon, (2/L) - \varepsilon]$ and L is the Lipschitz constant of $\nabla\wp$.

For machine learning tasks, where the dataset can be large, an algorithm that converges slowly is computationally expensive and impractical. Moreover, the standard algorithm requires the step size to be chosen based on the Lipschitz constant which is either unknown or very difficult to compute, creating a major implementation challenge.

To accelerate the convergence of sequence, Moudafi and Oliny [21] introduced the inertial proximal gradient method. In 2016, Cruz and Nghia [4] proposed a forward-backward algorithm using the linesearch technique (NFBMwL). This algorithm does not require the Lipschitz constant in computation.

Algorithm 2.1. Given $\sigma > 0, \theta \in (0,1)$ and $\delta \in (0, \frac{1}{2})$. Let $\phi^0 \in H$. For $n \geq 0$, calculate

$$\phi^{n+1} = \text{prox}_{\alpha_n \Im}(\phi^n - \alpha_n \nabla \wp(\phi^n)),$$

where $\alpha_n = \sigma\theta^{m_n}$ and m_n is the smallest nonnegative integer satisfying the following linesearch rule:

$$\alpha_n \|\nabla \wp(\phi^{n+1}) - \nabla \wp(\phi^n)\| \leq \delta \|\phi^{n+1} - \phi^n\|.$$

It was proved that the sequence (ϕ^n) converges weakly to a minimizer of $\wp + \Im$ under suitable conditions.

3. Main Theorem

According to the previous section, the practical task of classifying clay brick compressive strength can be rigorously modeled as the constrained convex minimization problem, we now introduce the main theoretical contribution of this work as an algorithm designed specifically for this class of problems.

This section, we assume that $\wp, \Im : H \to \mathbb{R} \cup \{+\infty\}$ are two proper, lower-semicontinuous and convex functions. The function $\wp$ is Fréchet differentiable on an open set containing H. The gradient $\nabla\wp$ is uniformly continuous on any bounded subset of H.

Linesearch 3.1. (Linesearch max) Given $\phi \in H$, $\sigma > 0$, $\theta \in (0,1)$and $\delta \in (0, 1/4)$.
Input. Set $\alpha = \sigma$, $L(\phi, \alpha) = \text{prox}_{\alpha\Im}(\phi - \alpha\nabla\wp(\phi))$ and $S(\phi, \alpha) = \text{prox}_{\alpha\Im}(L(\phi, \alpha) - \alpha\nabla\wp(L(\phi, \alpha)))$.

While

$$\begin{aligned} & \alpha \max\{\|\nabla\wp(S(\phi,\alpha)) - \nabla\wp(L(\phi,\alpha))\|, \|\nabla\wp(L(\phi,\alpha)) - \nabla\wp(\phi)\|\} \\ > \; & \delta(\|S(\phi,\alpha) - L(\phi,\alpha)\|, \|L(\phi,\alpha) - \wp(\phi)\|) \end{aligned}$$

do $\alpha = \theta\alpha$
End While
Output. α.

Lemma 3.2. [13] The Linesearch 3.1 stops after finitely many steps.

Using Lemma 3.2, we define the following algorithm with Linesearch 3.1.

Algorithm 3.3. Inertial projected forward-backward algorithm with Linesearch (IPFBAwL)
Initialization: Given $\theta > 0, \delta \in (0, 1/4)$, $\theta_n \in [0, \infty)$ and $\eta_n \in [0, 1]$.
Iterative step: Let $\phi^0, \phi^1 \in H$ and calculate ϕ^{n+1} as follows:
Step1. Compute the inertial step:

$$\rho^n = \phi^n + \theta_n(\phi^n - \phi^{n-1}) \text{ and } \varphi^n = \rho^n + \eta_n(\phi^n - \rho^n)$$

Step2. Compute the forward-backward step:

$$\psi^n = \text{prox}_{\alpha_n \Im}(\varphi^n - \alpha_n \nabla \wp(\varphi^n))$$

and

$$\omega^n = \text{prox}_{\alpha_n \Im}(\psi^n - \alpha_n \nabla \wp(\psi^n))$$

where $\alpha_n :=$ Linesearch max. If $\psi^n = \omega^n$ then stop. Otherwise, go to **Step 3**.
Step3. Compute the ϕ^{n+1} step:

$$\phi^{n+1} = P_\Omega(\omega^n).$$

Set $n := n + 1$ and return to **Step1.**

Theorem 3.4. Let (ϕ^n) be generated by Algorithm 3.3. Assume that $0 < \liminf_{n\to\infty} \alpha_n \leq \limsup_{n\to\infty} \alpha_n < \alpha$, $\sum_{n=1}^{\infty} \theta_n < +\infty$. Then we have

(1) for each $\phi^* \in \operatorname{argmin}(\wp + \Im) \cap \Omega$,

$$\|\phi^{n+1} - \phi^*\| \leq K \cdot \prod_{j=1}^{n}(1 + 2\theta_j),$$

where $K = \max\{\|\phi^0 - \phi^*\|, \|\phi^1 - \phi^*\|\}$.

(2) (ϕ^n) weakly converges to an element of $\operatorname{argmin}(\wp + \Im) \cap \Omega$.

Proof. Let $\phi^* \in \operatorname{argmin}(\wp + \Im) \cap \Omega$. So, we get

$$\begin{aligned} \|\phi^{n+1} - \phi^*\|^2 &= \|P_\Omega(\omega^n) - \phi^*\|^2 \\ &\leq \|\omega^n - \phi^*\|^2 - \|P_\Omega(\omega^n) - \omega^n\|^2. \end{aligned} \tag{3.1}$$

From definition of ω^n, we see that

$$\frac{\psi^n - \omega^n}{\alpha_n} - \nabla\wp(\psi^n) = \frac{\psi^n - \operatorname{prox}_{\alpha_n\Im}(\psi^n - \alpha_n\nabla\wp(\psi^n))}{\alpha_n} - \nabla\wp(\psi^n) \in \partial\Im(\omega^n).$$

It follows from the convexity of g, that

$$\Im(\phi^*) - \Im(\omega^n) \geq \langle \frac{\psi^n - \omega^n}{\alpha_n} - \nabla\wp(\psi^n), \phi^* - \omega^n\rangle. \tag{3.2}$$

Also, by definition of ψ^n, we get

$$\frac{\varphi^n - \psi^n}{\alpha_n} - \nabla\wp(\varphi^n) = \frac{\varphi^n - \operatorname{prox}_{\alpha_n\Im}(\varphi^n - \alpha_n\nabla\wp(\varphi^n))}{\alpha_n} - \nabla\wp(\varphi^n) \in \partial\Im(\psi^n)$$

and

$$\Im(\phi^*) - \Im(\psi^n) \geq \langle \frac{\varphi^n - \psi^n}{\alpha_n} - \nabla\wp(\varphi^n), \phi^* - \psi^n\rangle. \tag{3.3}$$

By the convexity of f, we get

$$\wp(\phi^*) - \wp(\psi^n) \geq \langle \nabla\wp(\psi^n), \phi^* - \psi^n\rangle \tag{3.4}$$

and

$$\wp(\phi^*) - \wp(\varphi^n) \geq \langle \nabla\wp(\varphi^n), \phi^* - \varphi^n\rangle. \tag{3.5}$$

So from (3.2), (3.3), (3.4) and (3.5), we have

$$\begin{aligned} &\Im(\phi^*) - \Im(\omega^n) + \Im(\phi^*) - \Im(\psi^n) + \wp(\phi^*) - \wp(\psi^n) + \wp(\phi^*) - \wp(\varphi^n) \\ \geq\ & \left\langle \frac{\psi^n - \omega^n}{\alpha_n} - \nabla\wp(\psi^n), \phi^* - \omega^n \right\rangle + \left\langle \frac{\varphi^n - \psi^n}{\alpha_n} - \nabla\wp(\varphi^n), \phi^* - \psi^n \right\rangle + \langle \nabla\wp(\psi^n), \phi^* - \psi^n\rangle \\ & + \langle \nabla\wp(\varphi^n), \phi^* - \varphi^n\rangle \\ =\ & \frac{1}{\alpha_n}\langle \psi^n - \omega^n, \phi^* - \omega^n\rangle + \frac{1}{\alpha_n}\langle \varphi^n - \psi^n, \phi^* - \psi^n\rangle + \langle \nabla\wp(\psi^n), \omega^n - \psi^n\rangle + \langle \nabla\wp(\varphi^n), \psi^n - \varphi^n\rangle \\ =\ & \frac{1}{\alpha_n}\langle \psi^n - \omega^n, \phi^* - \omega^n\rangle + \frac{1}{\alpha_n}\langle \varphi^n - \psi^n, \phi^* - \psi^n\rangle + \langle \nabla\wp(\psi^n) - \nabla\wp(\omega^n), \omega^n - \psi^n\rangle \\ & + \langle \nabla\wp(\omega^n), \omega^n - \psi^n\rangle + \langle \nabla\wp(\varphi^n) - \nabla\wp(\psi^n), \psi^n - \varphi^n\rangle + \langle \nabla\wp(\psi^n), \psi^n - \varphi^n\rangle. \end{aligned}$$

By the convexity of f, we get

$$\begin{aligned} &\Im(\phi^*) - \Im(\omega^n) + \Im(\phi^*) - \Im(\psi^n) + \wp(\phi^*) - \wp(\psi^n) + \wp(\phi^*) - \wp(\varphi^n) \\ \geq\ & \frac{1}{\alpha_n}[\langle \psi^n - \omega^n, \phi^* - \omega^n\rangle + \langle \varphi^n - \psi^n, \phi^* - \psi^n\rangle] - \|\nabla\wp(\psi^n) - \nabla\wp(\omega^n)\|\|\omega^n - \psi^n\| \\ & + \wp(\omega^n) - \wp(\psi^n) - \|\nabla\wp(\varphi^n) - \nabla\wp(\psi^n)\|\|\psi^n - \varphi^n\| + \wp(\psi^n) - \wp(\varphi^n). \end{aligned}$$

By Linesearch, we obtain

$$\begin{aligned}
&\frac{1}{\alpha_n}[\langle \psi^n-\omega^n,\omega^n-\phi^*\rangle+\langle \varphi^n-\psi^n,\psi^n-\phi^*\rangle]\\
\geq\ & (\wp+\Im)(\omega^n)-(\wp+\Im)(\phi^*)+(\wp+\Im)(\psi^n)-(\wp+\Im)(\phi^*)-\|\nabla\wp(\psi^n)-\nabla\wp(\omega^n)\|\|\omega^n-\psi^n\|\\
&-\|\nabla\wp(\varphi^n)-\nabla\wp(\psi^n)\|\|\psi^n-\varphi^n\|\\
\geq\ & (\wp+\Im)(\omega^n)-(\wp+\Im)(\phi^*)+(\wp+\Im)(\psi^n)-(\wp+\Im)(\phi^*)\\
&-\max(\|\nabla\wp(\psi^n)-\nabla\wp(\omega^n)\|,\|\nabla\wp(\varphi^n)-\nabla\wp(\psi^n)\|)\|\omega^n-\psi^n\|\\
&-\max(\|\nabla\wp(\psi^n)-\nabla\wp(\omega^n)\|,\|\nabla\wp(\varphi^n)-\nabla\wp(\psi^n)\|)\|\psi^n-\varphi^n\|\\
\geq\ & (\wp+\Im)(\omega^n)-(\wp+\Im)(\phi^*)+(\wp+\Im)(\psi^n)-(\wp+\Im)(\phi^*)\\
&-\frac{\delta}{\alpha_n}(\|\omega^n-\psi^n\|+\|\varphi^n-\psi^n\|)\|\psi^n-\varphi^n\|-\frac{\delta}{\alpha_n}(\|\omega^n-\psi^n\|+\|\varphi^n-\psi^n\|)\|\psi^n-\varphi^n\|\\
\geq\ & (\wp+\Im)(\omega^n)-(\wp+\Im)(\phi^*)+(\wp+\Im)(\psi^n)-(\wp+\Im)(\phi^*)\\
&-\frac{\delta}{\alpha_n}\|\omega^n-\psi^n\|^2-\frac{2\delta}{\alpha_n}\|\varphi^n-\psi^n\|\|\psi^n-\varphi^n\|-\frac{\delta}{\alpha_n}\|\psi^n-\varphi^n\|^2\\
\geq\ & (\wp+\Im)(\omega^n)-(\wp+\Im)(\phi^*)+(\wp+\Im)(\psi^n)-(\wp+\Im)(\phi^*)\\
&-\frac{\delta}{\alpha_n}\|\omega^n-\psi^n\|^2-\frac{\delta}{\alpha_n}(\|\varphi^n-\psi^n\|^2+\|\psi^n-\varphi^n\|^2)-\frac{\delta}{\alpha_n}\|\psi^n-\varphi^n\|^2\\
\geq\ & (\wp+\Im)(\omega^n)-(\wp+\Im)(\phi^*)+(\wp+\Im)(\psi^n)-(\wp+\Im)(\phi^*)-\frac{2\delta}{\alpha_n}\|\omega^n-\psi^n\|^2-\frac{2\delta}{\alpha_n}\|\psi^n-\varphi^n\|^2.
\end{aligned}$$

We know that $\pm 2\langle a,b\rangle=\|a\|^2+\|b\|^2-\|a\pm b\|^2$ for all $a,b\in H$. So, we have

$$\begin{aligned}
\|\omega^n-\phi^*\|^2 \leq\ & \|\varphi^n-\phi^*\|^2-2\alpha_n[(\wp+\Im)(\omega^n)-(\wp+\Im)(\phi^*)+(\wp+\Im)(\psi^n)-(\wp+\Im)(\phi^*)]\\
&-(1-4\delta)\|\psi^n-\omega^n\|^2-(1-4\delta)\|\varphi^n-\psi^n\|^2
\end{aligned}\tag{3.6}$$

By (3.1) and (3.6), we see that

$$\begin{aligned}
\|\phi^{n+1}-\phi^*\| &\leq \|\varphi^n-\phi^*\|\\
&= \|\rho^n+\eta_n(\phi^n-\rho^n)\|\\
&= \|\eta_n(\phi^n-\phi^*)+(1-\eta_n)(\rho^n-\phi^*)\|\\
&\leq \eta_n\|\phi^n-\phi^*\|+(1-\eta_n)\|\phi^n-\phi^*+\theta_n(\phi^n-\phi^{n-1})-\phi^*\|\\
&\leq \|\phi^n-\phi^*\|+\theta_n\|\phi^n-\phi^{n-1}\|\\
&\leq \|\phi^n-\phi^*\|+\theta_n(\|\phi^n-\phi^*\|+\|\phi^{n-1}-\phi^*\|).
\end{aligned}$$

This shows that

$$\|\phi^{n+1}-x_*\|\leq(1+\theta_n)\|\phi^n-x_*\|+\theta_n\|\phi^{n-1}-x_*\|.$$

By Lemma 5 in [9], we can conclude that

$$\|\phi^{n+1}-x_*\|\leq K\cdot\prod_{j=1}^{n}(1+2\theta_j)$$

where $K = \max\{\|\phi^0 - x_*\|, \|\phi^1 - x_*\|\}$. Since $\sum_{n=1}^{\infty} \theta_n < +\infty$, we get (ϕ^n) is bounded. So, we have

$$\begin{aligned}
\|\phi^{n+1} - x_*\|^2 &\leq (\|\phi^n - x_*\| + \theta_n\|\phi^n - \phi^{n-1}\|)^2 - 2\alpha_n[(\wp + \Im)(\omega^n) - (\wp + \Im)(\phi^*) + (\wp + \Im)(\psi^n) \\
&\quad -(\wp + \Im)(\phi^*)] - (1 - 4\delta)\|\psi^n - \omega^n\|^2 - (1 - 4\delta)\|\varphi^n - \psi^n\|^2 \\
&= \|\phi^n - x_*\|^2 + \theta_n^2\|\phi^n - \phi^{n-1}\|^2 + 2\theta_n\|\phi^n - x_*\|\|\phi^n - \phi^{n-1}\| \\
&\quad -2\alpha_n[(\wp + \Im)(\omega^n) - (\wp + \Im)(\phi^*) + (\wp + \Im)(\psi^n) - (\wp + \Im)(\phi^*)] \\
&\quad -(1 - 4\delta)\|\psi^n - \omega^n\|^2 - (1 - 4\delta)\|\varphi^n - \psi^n\|^2.
\end{aligned}$$

Since $\lim_{n\to\infty} \theta_n(\phi^n - \phi^{n-1}) = 0$, $\lim_{n\to\infty} \|\phi^n - x_*\|$ exist and $1 - 4\delta > 0$, we have

$$\lim_{n\to\infty} \|\omega^n - \psi^n\| = 0 \text{ and } \lim_{n\to\infty} \|\varphi^n - \psi^n\| = 0.$$

By definition of ρ^n, we have $\lim_{n\to\infty} \|\rho^n - \rho^n\| = 0$. Then

$$\begin{aligned}
\|\varphi^n - \phi^n\| &\leq (1 - \eta_n)\|\rho^n - \phi^n\| \\
&\leq \|\rho^n - \phi^n\| \\
&= \theta_n\|\phi^n - \phi^{n-1}\| \\
&\to 0 \text{ as } n \to \infty.
\end{aligned}$$

Moreover, we have

$$\|\psi^n - \phi^n\| = \|\psi^n - \varphi^n\| + \|\varphi^n - \phi^n\| \to 0 \text{ as } n \to \infty.$$

Since the sequence (ϕ^n) is bounded, let (ϕ^{n_i}) be a subsequence of (ϕ^n) such that $\phi^{n_i} \rightharpoonup \phi^\infty$. Since $\lim_{i\to\infty} \|\psi^{n_i} - \phi^{n_i}\| = 0$, we also obtain $\psi^{n_i} \rightharpoonup \phi^\infty$ as $i \to \infty$. Since (ψ^{n_i}) is bounded, $\lim_{i\to\infty} \|\psi^{n_i} - \varphi^{n_i}\| = 0$ and $\nabla\wp$ is uniformly continuous on H, we have

$$\lim_{n\to\infty} \|\nabla\wp(\psi^{n_i}) - \nabla\wp(\varphi^{n_i})\| = 0.$$

By definition ψ^{n_i}, we see that

$$\begin{aligned}
\frac{\varphi^{n_i} - \psi^{n_i}}{\alpha_{n_i}} - \nabla\wp(\varphi^{n_i}) &= \frac{\varphi^{n_i} - \text{prox}_{\alpha_{n_i}\Im}(\varphi^{n_i} - \alpha_{n_i}\nabla\wp(\varphi^{n_i})) - \alpha_{n_i}\nabla\wp(\varphi^{n_i})}{\alpha_{n_i}} \\
&\in \partial\Im(\psi^{n_i}).
\end{aligned}$$

It follows that

$$\begin{aligned}
\frac{\varphi^{n_i} - \psi^{n_i}}{\alpha_{n_i}} + \nabla\wp(\psi^{n_i}) - \nabla\wp(\varphi^{n_i}) &\in \nabla\wp(\psi^{n_i}) + \partial\Im(\psi^{n_i}) \\
&\subseteq \partial(\wp + \Im)(\psi^{n_i}).
\end{aligned}$$

By passing $i \to \infty$ and using Face 2.2 in [4], we have $0 \in \nabla\wp(\phi^\infty) + \partial\Im(\phi^\infty)$. Thus $\phi^\infty \in \text{argmin}(\wp + \Im)$. On the other hand, since $\lim_{n\to\infty} \|P_\Omega(\omega^n) - \omega^n\| = 0$ and $\omega^n \to \phi^\infty$. By the definition of the projection, we have $\phi^\infty \in \Omega$. Therefore $\phi^\infty \in \Omega \cap \text{argmin}(\wp + \Im)$. Using Theorem 5.5 in [3], we conclude that this theorem holds. □

The theorem provides the essential guarantee that the method is sound and will reliably converge to a correct solution, becoming a robust and trustworthy tool with its proof. Without this proof, the algorithm is merely a heuristic. This result is the critical link between our theoretical framework and practical application, ensuring that the computational method used to train our brick classifier is not an ad hoc procedure but a mathematically validated process. This is the theoretical justification for the experimental results that will follow.

4. Numerical Experiments

The numerical experiment's dataset comprises 95 instances, consisting of an experimental dataset with seven attributes. These attributes include input parameters such as firing temperature, amount, and size of additive, as well as physical properties such as apparent porosity, bulk density, and water absorption. These phenomena are hypothesized to be used to predict the mechanical characteristic of materials as compressive strength. The overview of the data is shown in the Table 1.

Table 1. Distribution of features for compressive strength classification

Attribute name	Description	Value type	Variable type
FT	Firing Temperature in Degree Celsius	int (°C)	Objective
AA	Amount of Additive in Percentage by Weight	int (%wt)	
AS	Size of Additive in Millimeter	int (mm.)	
FS	Firing Shrinkage in Percentage	int (%)	
BD	Bulk Density in Percentage	int (g/cm^3)	
WA	Water Absorption in Percentage	int (%)	
AP	Apparent Porosity in Percentage	int (%)	
CS	Presence Compressive Strength of (Mpa)	Categorucal Code	Target

According to Table 1, the firing temperature (FT) denotes the specific temperature at which clay bricks undergo the heating phase in the firing process. The experimental firing temperature is measured in degrees Celsius. The amount of additive (AA) pertains to the quantity or ratio of supplementary substance introduced into the clay mixture during brick production. The amount of additive utilized in this experiment is expressed as a weight percentage. Additionally, the particle size of the additive (AS) demonstrates to the range or distribution of particles within the additive material. In this experiment, the size is measured and expressed in millimeters using average particle size units.

Moreover, the firing shrinkage (FS) pertains to the dimensional or volumetric reduction that occurs in clay bricks due to the firing process. This phenomenon can be attributed to various factors, such as the evaporation of moisture, the combustion of organic matter, and the reconfiguration of particles induced by elevated temperatures.

Next, bulk density (BD) is a quantitative measure that expresses the mass of a substance concerning its volume, encompassing the interstitial voids between individual particles. The parameter denotes the degree of particle density within a specified volume. The experimental procedure employs the metric unit of grams per cubic centimeter (g/cm^3) to measure bulk density. The next attribute is water absorption (WA), referring to the capacity of a substance to take in and retain water when submerged in or exposed to moisture. The metric is quantified as a proportion, represented as a percentage, denoting

the amount of water absorbed with the weight of the material when it is devoid of moisture. The property of water absorption significantly influences the assessment of material durability.

The apparent porosity (AP) indicates the proportion of void spaces or pores within a material, expressed as a percentage of its overall volume. Those mentioned above characteristic denotes the material's open or closed porosity, which in turn influences its permeability and propensity for water absorption. Determining apparent porosity involves measuring the water volume absorbed by a given sample, which is then compared to the total volume of the sample.

To perform the numerical experiment of our algorithm, we let $S := \{(\psi^n, \flat^n) | \psi^n \in \mathbb{R}^q, \flat^n \in \mathbb{R}^p, n = 1, 2, ..., J\}$ be the training dataset, where J is distinct samples, ψ^n is an input data and $\flat^n$ is a target. In experiments on regression and classification problems, the main goal of extreme learning machine (ELM) is to find

$$\phi = [{\phi^1}^T, ..., {\phi^M}^T]^T \text{ such that } \Delta\phi = \flat$$

where M is number of nodes in the hidden layer and Δ is hidden layer output matrix defied by

$$\Delta = \begin{bmatrix} \eth(a^1\psi^1 + \flat^1) & \cdots & \eth(a^M\psi^1 + \flat^M) \\ \vdots & \ddots & \vdots \\ \eth(a^1\psi^K + \flat^1) & \cdots & \eth(a^M\psi^K + \flat^M) \end{bmatrix},$$

$\eth$ is an activate function, a^i and $\flat^i$ are random weight and bias of the i-th hidden node and $\flat = [{\flat^1}^T, ..., {\flat^J}^T]^T$ is the training data. The output at the $i-$th hidden node is

$$O^n = \sum_{i=1}^{M} \phi^i \Im(a^i\psi^n + \flat^i).$$

The classification problems for regularized the least square problem to get the good fit model of our algorithm can be expressed in Table 2.

TABLE 2. List of models considered for the proposed algorithm

Models	**Function**	**Explanation**	**Argument**
M1	$\text{prox}_{\ell 1}$	ℓ_1 norm proximal operator. Solve: $\min_{\phi \in H} \|\Delta\phi - \flat\|_2^2 + \lambda\|\phi\|_1$	ϕ, λ, parameters
The problem (2.3) setting: $\wp(\phi) = \|\Delta\phi - \flat\|_2^2$ and $\Im(\phi) = \lambda\|\phi\|_1$.			
M2	$\text{prox}_{\ell 2}$	ℓ_2 norm proximal operator. Solve: $\min_{\phi \in H} \|\Delta\phi - \flat\|_2^2 + \lambda\|\phi\|_2^2$	ϕ, λ, parameters
The problem (2.3) setting: $\wp(\phi) = \|\Delta\phi - \flat\|_2^2$ and $\Im(\phi) = \lambda\|\phi\|_2^2$.			
M3	$\text{prox}_{\ell 1}$	ℓ_1 norm proximal operator. Solve: $\min_{\phi \in C} \|\Delta\phi - \flat\|_2^2 + \lambda_1\|\phi\|_1$	$\phi, \lambda_1, \lambda_2$, parameters
The problem (2.1) setting: $\wp(\phi) = \|\Delta\phi - \flat\|_2^2$, $\Im(\phi) = \lambda\|\phi\|_1$ and $C = \{\phi \in \mathbb{R} \mid \|\phi\|_1 < \lambda_2\}$.			
M4	$\text{prox}_{\ell 2}$	ℓ_2 norm proximal operator. Solve: $\min_{\phi \in C} \|\Delta\phi - \flat\|_2^2 + \lambda_1\|\phi\|_2^2$	$\phi, \lambda_1, \lambda_2$, parameters
The problem (2.1) setting: $\wp(\phi) = \|\Delta\phi - \flat\|_2^2$, $\Im(\phi) = \lambda\|\phi\|_2^2$ and $C = \{\phi \in \mathbb{R} \mid \|\phi\|_2^2 < \lambda_2\}$.			

Where λ, λ_1 and λ_2 are a regularization parameter.

To predict compressive strength, we apply the proposed algorithm to solve all models in Table 2. All results are performed by MATLAB 2022b on a MacBook Pro Chip Apple M1 64-bit and 8 GB of RAM. To evaluate the quality of the predicted dataset, we use precision, recall, F1 score and accuracy, which are defined by

$$\textbf{precision}\ (\mathrm{PRE}) = \frac{\mathrm{TP}}{\mathrm{TP}+\mathrm{FP}},$$

$$\textbf{recall}\ (\mathrm{REC}) = \frac{\mathrm{TP}}{\mathrm{TP}+\mathrm{FN}},$$

$$\textbf{F1 score}\ (\mathrm{F1}) = \frac{2\mathrm{TP}}{2\mathrm{TP}+\mathrm{FP}+\mathrm{FN}}$$

and

$$\textbf{accuracy}\ (\mathrm{ACC}\%) = \frac{\mathrm{TP}+\mathrm{TN}}{\mathrm{TP}+\mathrm{FP}+\mathrm{TN}+\mathrm{FN}} \times 100\%,$$

where TP is a true positive, TN is a true negative, FP is a false positive and FN is false negative. The multi-class cross entropy loss function calculates the loss of an example by computing the following average:

$$\mathrm{Loss} = -\sum_{i=1}^{\text{output size}} \psi_i \log \bar{\psi}_i,$$

where output size is the number of scalar values in the model output, ψ_i is a corresponding target value and $\bar{\psi}_i$ is a ith scalar value in the model output.

The dataset contains 95 samples, seven experimental features of materials for predicting the compressive strength with statistical description as in Table 3. 70% of the dataset was selected as the training set and 30% as the test set to cross-validate the model's performance, and adjust the classification model according to the parameters of the classification algorithm.

TABLE 3. Statistical description of the balanced data

Attribute name	Maximum (Minimum)	Mean	Standard Deviation (SD)
FT	1150 (950)	1050	71.0858
AA	30 (0)	16.5789	9.2329
AS	2 (0)	1.1053	0.6640
FS	21.72 (9.42)	14.8064	2.8895
BD	2.01 (0.96)	1.4618	0.2784
WA	72.84 (0.31)	32.9663	16.1633
AP	51.63 (8.12)	27.9432	9.8247

The initial points $\phi^0 = \phi^1$ are zero vectors with the size of training dataset for all algorithms. θ_n of Algorithms 3.3 (IPFBAwL) is defined as

$$\theta_n = \begin{cases} \dfrac{t_n - 1}{t_{n+1}} \text{ where } t_{n+1} = \dfrac{1+\sqrt{1+4t_n^2}}{2}, & \text{if } 1 \le n \le M; \\ \dfrac{1}{n^2}, & \text{otherwise,} \end{cases} \tag{4.1}$$

for some positive integer M and $\eta_n = 0.4$. The sigmoid vis an activation function, hidden nodes $M = 225$, and the binary cross entropy loss = 0.015 for the stopping criteria. The results as shown in Table 5.

TABLE 4. Chosen regularization parameters of each algorithm

Models	Regularization parameters		
	$\lambda = 10^{-4}$	$\lambda_1 = 10^{-4}$	$\lambda_2 = 0.4$
M1	✓	–	–
M2	✓	–	–
M3	–	✓	✓
M4	–	✓	✓

The accuracy and the other performance measures of different attributes are recorded in Table 5 and Table 6.

TABLE 5. The performance for solving model M2

Choose attribute	ITER (CPU)	PRE/REC/F1	ACC(%)
All	250 (0.1849)	59.2593	83.7037
Exclude FT	250 (0.1490)	66.6667	86.6667
Exclude AA	250 (0.1471)	70.3704	88.1481
Exclude AS	250 (0.1913)	62.9630	85.1852
Exclude FS	250 (0.1479)	66.6667	86.6667
Exclude BD	250 (0.1630)	62.9630	85.1852
Exclude WA	250 (0.2246)	51.8519	80.7407
Exclude AP	250 (0.1816)	66.6667	86.6667

The findings presented in Table 5 indicate that our algorithm, when utilizing six attributes excluding the amount of additive, outperforms the use of seven features with an accuracy rate of 88.15%. Furthermore, all cases, with the exception of firing temperature, firing shrinkage, and apparent porosity, exhibit an equivalent level of accuracy, specifically 86.67%. In instances where six attributes are utilized, with the exception of additive sizes and bulk density, the performances demonstrate an equivalent level of accuracy, specifically 85.19%. In addition, our algorithm achieved a relatively low accuracy of 80.74% when utilizing six attributes, excluding the water absorption property.

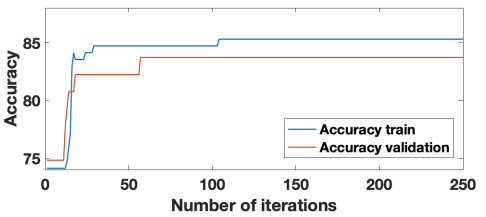

(A) Accuracy plots of training and validation

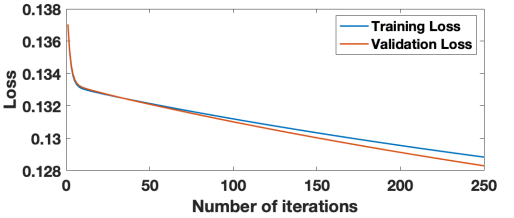

(B) Loss plots of training and validation

FIGURE 1. Training and accuracy, and the validation loss plots of Algorithm 3.3 (IPFBAwL) with model M2 for all attributes, respectively.

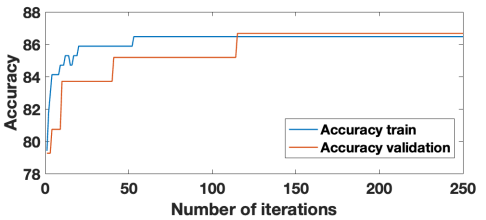

(A) Accuracy plots of training and validation

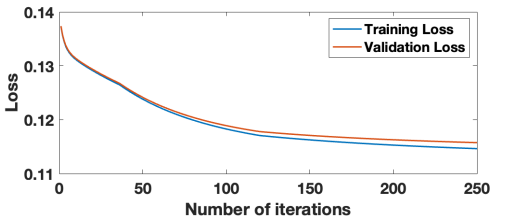

(B) Loss plots of training and validation

FIGURE 2. Training and accuracy, and the validation loss plots of Algorithm 3.3 (IPFBAwL) for all attributes except temperature, respectively.

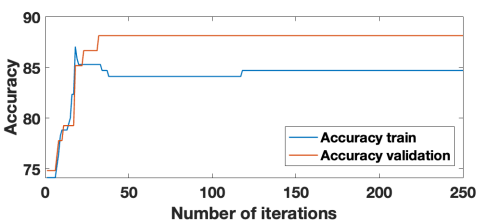

(A) Accuracy plots of training and validation

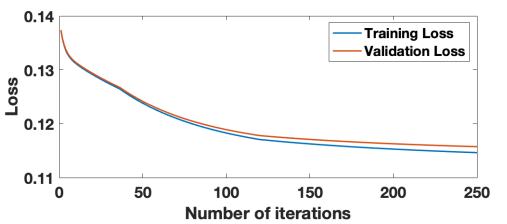

(B) Loss plots of training and validation

FIGURE 3. Training and accuracy, and the validation loss plots of Algorithm 3.3 (IPFBAwL) for all attributes except addition, respectively.

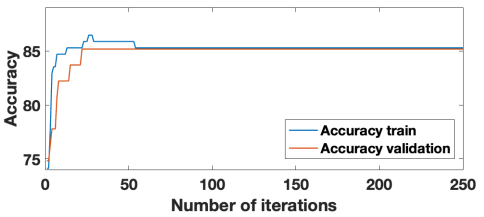

(A) Accuracy plots of training and validation

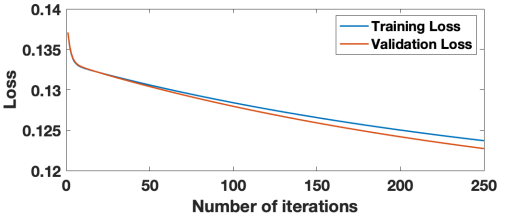

(B) Loss plots of training and validation

FIGURE 4. Training and accuracy, and the validation loss plots of Algorithm 3.3 (IPFBAwL) for all attributes except add size, respectively.

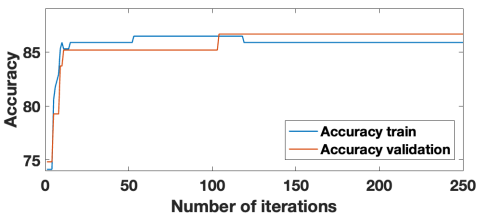

(A) Accuracy plots of training and validation

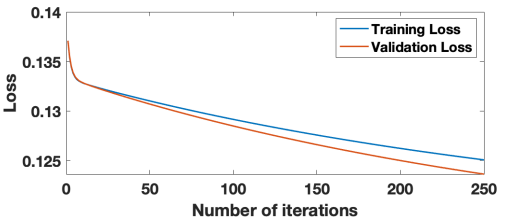

(B) Loss plots of training and validation

FIGURE 5. Training and accuracy, and the validation loss plots of Algorithm 3.3 (IPFBAwL) for all attributes except FS, respectively.

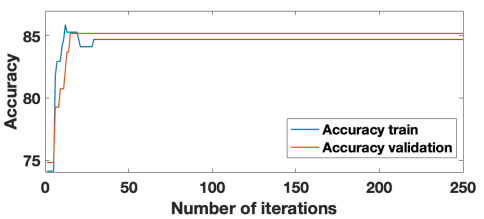

(A) Accuracy plots of training and validation

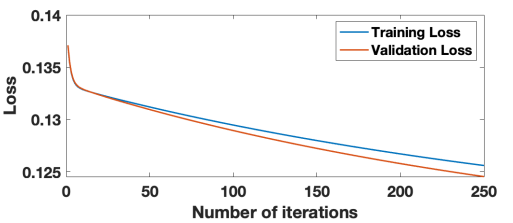

(B) Loss plots of training and validation

FIGURE 6. Training and accuracy, and the validation loss plots of Algorithm 3.3 (IPFBAwL) for all attributes except BD, respectively.

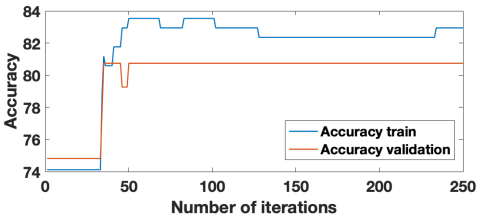

(A) Accuracy plots of training and validation

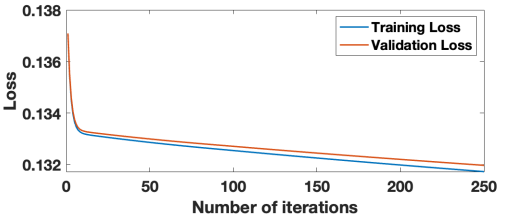

(B) Loss plots of training and validation

FIGURE 7. Training and accuracy, and the validation loss plots of Algorithm 3.3 (IPFBAwL) for all attributes except WT, respectively.

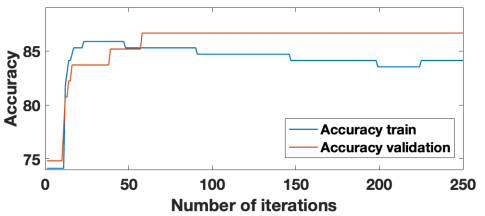

(A) Accuracy plots of training and validation

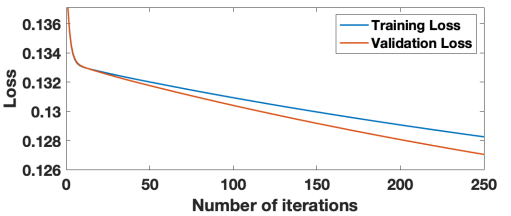

(B) Loss plots of training and validation

FIGURE 8. Training and accuracy, and the validation loss plots of Algorithm 3.3 (IPFBAwL) for all attributes except AP, respectively.

From Figures 1-8, we see that Algorithm 3.3 (IPFBAwL) has an optimal-fitting model this means that our algorithm suitably learns the training dataset and generalizes well to predict the compressive strength dataset.

TABLE 6. Numerical results of training-validation loss and training time

Models (⇒)	**M1**		**M2**		**M3**		**M4**	
Choose attribute	**CPU**	**LOSS**	**CPU**	**LOSS**	**CPU**	**LOSS**	**CPU**	**LOSS**
(⇓)		**Training (Validation)**		**Training (Validation)**		**Training (Validation)**		**Training (Validation)**
All	0.1999	0.1240 (0.1227)	0.1857	0.1288 (0.1283)	0.0963	1.1187 (0.1162)	0.1467	0.1288 (0.1283)
Except Temp	0.1163	0.1087 (0.1109)	0.1714	0.1146 (0.1157)	0.1183	0.1066 (0.1092)	0.3219	0.1146 (0.1157)
Except Additive	0.1214	0.1221 (0.1173)	0.1601	0.1272 (0.1246)	0.0972	0.1173 (0.1107)	0.1367	0.1272 (0.1246)
Except Add_size	0.1195	0.1185 (0.1170)	0.1572	0.1237 (0.1227)	0.1006	0.1129 (0.1110)	0.1492	0.1237 (0.1227)
Except FS	0.1927	0.1202 (0.1179)	0.1681	0.1251 (0.1236)	0.0997	0.1152 (0.1122)	0.1966	0.1251 (0.1236)
Except BD	0.1203	0.1204 (0.1190)	0.1811	0.1256 (0.1245)	0.0956	0.1149 (0.1142)	0.1684	0.1256 (0.1245)
Except WT	0.1235	0.1277 (0.1284)	0.2449	0.1317 (0.1320)	0.1513	0.1259 (0.1268)	0.1893	0.1317 (0.1320)
Except AP	0.1106	0.1231 (0.1208)	0.1146	0.1282 (0.1270)	0.0909	0.1167 (0.1135)	0.2665	0.1282 (0.1270)

The initial points $\phi^0 = \phi^1$ are zero vectors with the size of training dataset for all algorithms. The parameter $\alpha_n = \dfrac{0.21}{\max(\mathrm{eig}(\Delta^T\Delta))}$ where $\mathrm{eig}(\Delta^T\Delta)$ is eigenvalues of $\Delta^T\Delta$. The parameter θ_n of Algorithm (OUR) is defined by (4.1) for some positive integer M and $\eta_n = 0.4$.

TABLE 7. Chosen parameters of each algorithm

Methods	**Parameters**				
	$\alpha = \dfrac{0.21}{\max(\mathrm{eig}(\Delta^T\Delta))}$	$\sigma =$ 0.91	$\theta =$ 0.69	$\delta =$ 0.23	$\eta =$ 0.90
FBS-CW	✓	–	–	–	–
NFBMwL	–	✓	✓	✓	–
IPFBAwL	–	✓	✓	✓	✓

Next experiment, we compare the performance of FBS-CW, NFBMwL and our algorithm (IPFBAwL). We choose the same parameters as in Table 7. As shown in Table 8, this dataset contains 5 categories of 59 instances and each sample contains 7 attributes. The stopping criteria of training is ACC.train > 85 and ACC.test > 82, the results can be seen in Table 8.

TABLE 8. The best performance of each algorithm for comparison

Methods				**LOSS**	
	ITER	**PRE/REC/F1**	**ACC%**	Training	Validation
FBS-CW	52	59.2593	83.7037	0.1311	0.1309
NFBMwL	38	59.2593	83.7037	0.1314	0.1312
IPFBAwL	23	59.2593	83.7037	0.1331	0.1332

From Table 8, we see that Algorithm 3.3 has also high average accuracy compared other methods. Algorithm 3.3 are among those with the high precision, recall, and accuracy efficiency. However, it has the lowest number of iterations. It has optimal fitting in training.

The numerical results presented in this section provide strong quantitative evidence for the efficacy of our proposed algorithm. The accuracy and loss plots consistently demonstrate that our method achieves a faster convergence rate and superior classification accuracy compared to established benchmark algorithms.

Although these results are compelling from an optimization standpoint, their true value lies in their practical application. We will address the questions of how this enhanced performance translate into a more reliable and practical tool for the non-destructive classification of clay brick compressive strength. The following section will explore the broader implications of our findings.

5. DISCUSSION IN REAL-WORLD APPLICATION

Recently, there has been a surge in the utilization of machine learning algorithms and data-driven methodologies across diverse scientific and engineering fields [8, 7]. These techniques present considerable potential in augmenting various materials' classification and prediction capabilities [19, 30]. Establishing dependable and practical algorithms for the classification of compressive strength can bring about a significant transformation in

the clay bricks industry. This could facilitate the ability of manufacturers, engineers, and researchers to make well-informed decisions and enhance their processes.

In our study, according to Table 5, water absorption (WA) is a critical parameter in the algorithm, as its exclusion from the predictive parameters significantly reduces accuracy from 83.7037% to 80.7407%. This underscores the essential nature of WA relavant to many standards. Standards like ASTM (American Society for Testing and Materials) and TIS (Thai Industrial Standards) [29, 2] consistently incorporate WA to compressive strength (CS) as crucial parameters. Particularly, WA and CS exhibit an inverse relationship, where increasing WA tends to decrease CS. Bricks with higher WA typically possess greater porosity and more interconnected voids, compromising the structural integrity and lowering their CS. The significant relationship between WA and CS highlights the necessity of taking WA into account when prioritizing CS [5, 17].

Table 5 also demonstrates the relationship between additive size (AS) and bulk density (BD) indicates a potential correlation. While AS and BD exhibit exactly the same accuracy of 85.1852% when we excluded both attributes from the objective variables, suggesting a connection between the two parameters. Their relationship can be explained by the impact of additive size on the arrangement of clay particles. The smaller size of the additive particles can more effectively occupy the interstitial spaces between larger clay particles, leading to a denser packing arrangement. During the firing process, the additive burns out, allowing the clay particles to move closer together [16, 23]. Conversely, larger additive particles create empty spaces within the clay bricks as the clay particles struggle to reposition themselves, ultimately contributing to lower bulk density.

In Table5, the other relative attributes are firing temperature (FT), firing shrinkage (FS), and apparent porosity (AP), which are the same accuracy of 86.6667% when exclude for one of the attributes. This outcome from the numerical experiment of our algorithm compels us to investigate more into the experimental phenomena in our laboratory. We found that higher firing temperatures often reduce apparent porosity and increase firing shrinkage due to increased particle rearrangement and compaction, similar to results from many laboratory tests [22, 20]. Furthermore, as FT increases, some results found that clay particles undergo greater particle rearrangement and densification, resulting in increased FS [23, 22]. Particularly, higher FT generally promote denser packing of clay particles, reducing the overall porosity.

In conclusion, for future predictions of clay brick compressive strength using machine learning, the firing temperature alone suffices as a predictor, eliminating the requirement to gather data on firing shrinkage and apparent porosity.

Finally, the exclusion of the amount of additive (AA) from Table5 achieves its utmost accuracy of 88.1481%, leaving us with a peculiar phenomena. The result we have obtained shows that the amount of additive in the sample is not necessary for predicting the compressive strength of clay bricks. The AA directly affects compressive strength by reflected in other variables (AS, BD, WA, AP).

Thus, the result for numerical experiment of our algorithm shows that AA introduces multicollinearity and noise due to its strong correlation with other features and high variance in a small dataset, relevant to the result from [18]. Removing it reduces redundancy, improves generalization, and increases model accuracy.

The implications of the research results hold immense significance for the clay brick manufacturing industry, construction sector, and materials research community. The precise classification of clay bricks according to their compressive strength has the potential to enhance quality control, optimize material selection, improve the structural design and reduce industrial waste after empirical testing. Furthermore, our proposed algorithm has been suggested to exhibit the possibility of being expanded to other problems related to

material classification. This could lead to the progression of machine learning methodologies in the field of materials science and engineering.

6. Conclusion

The primary contribution of this work is twofold. First, on a theoretical level, we proposed a new inertial projected forward-backward algorithm to solve a constrained convex minimization problem (2.1). We have proved that the sequence generated by the algorithm weakly converges to a minimizer under some mild conditions. Our result can be applied effectively to solve data classification problems, as shown in numerical experiments. Comparison experiments showed that the proposed algorithm has a better efficiency than other comparison methods.

Second, we bridge the gap between theory and practice by applying our algorithm to the specific real-world problem of classifying the compressive strength of clay bricks. We can derive three principal conclusions from our numerical experiment. Firstly, the primary parameter influencing the prediction of compressive strength in clay bricks is its water absorption (WA), which results in the most significant decrease in forecast accuracy, from 83.7037 to 80.7407. Secondly, firing temperature (FT), firing shrinkage (FS), and apparent porosity (AP) exhibit identical accuracy of 86.6667%, indicating that for future forecasts of clay brick compressive strength using machine learning, FT alone is sufficient as a predictor, negating the need to collect data on FS and AP. Finally, the exclusion of the amount of additive (AA) from parameters results in a maximum accuracy of 88.1481%, surpassing the accuracy achieved when AA was included among the predictors of 83.7037%. Consequently, eliminating AA lowers redundancy, enhances generalization, and elevates model correctness.

This application serves not merely as a peripheral example, but as a core validation of our algorithm's efficacy and relevance. By demonstrating its superior performance on this practical engineering problem, we show that our theoretical advances translate into tangible improvements for solving complex, real-world classification tasks.

Acknowledgments

N. Jun-on and S. Lawanwadeekul would like to thank Thailand Science Research and Innovation, 2025 Fundamental Fund, Lampang Rajabhat University (Grant No. 030/2568).

K. Kankam, W. Cholamjiak and P. Cholamjiak would like to thank Thailand Science Research and Innovation, the University of Phayao (Grant No. FF68-UoE).

References

[1] Al-Fakih A.; Mohammed B. S.; Liew M. S.; Nikbakht E. Incorporation of waste materials in the manufacture of masonry bricks: An update review. *J. Build. Eng.* **21** (2019), no. 1, 37–54.

[2] ASTM C62-17. *Standard Specification for Building Brick (Solid Masonry Units Made From Clay or Shale)*. First edition. ASTM Book of Standards, 2017. West Conshohocken, Pennsylvania, 2017.

[3] Bauschke, H. H. and Combettes, P. L. *Convex Analysis and Monotone Operator Theory in Hilbert Spaces*. Second edition. Springer, New York, 2011.

[4] Bello Cruz, J. Y.; Nghia, T. T. On the convergence of the forward-backward splitting method with linesearches. *Optim. Methods Softw.* **31** (2016), no. 6, 1209–1238.

[5] Chindaprasirt P.; Srisuwan A.; Saengthong C.; Lawanwadeekul S.; Phonphuak, N. Synergistic effect of fly ash and glass cullet additive on properties of fire clay bricks. *J. Build. Eng.* **44** (2021), 102942.

[6] Combettes, P. L.; Wajs, V. R. Signal recovery by proximal forward-backward splitting. *Multiscale Model Sim.* **4** (2020), no. 4, 1168–1200.

[7] Garcia J.; Villavicencio G.; Altimiras F.; Crawford B.; Soto R.; Minatogawa V.; Yepes, V. Machine learning techniques applied to construction: A hybrid bibliometric analysis of advances and future directions. *Autom. Constr.* **142** (2022), 104532.

[8] Ghaffar S. H.; Corker J.; Fan M. Additive manufacturing technology and its implementation in construction as an eco-innovative solution. *Autom. Constr.* **93** (2020), 1–11.
[9] Hanjing, A., and Suantai, S. A fast image restoration algorithm based on a fixed point and optimization method. *Mathematics.* **8** (2020), no. 3, 378.
[10] Ishikawa, S. Fixed points by a new iteration method. *Proc. Am. Math. Soc.* **44** (1974), no. 1, 147–150.
[11] Kankam, K.; Cholamjiak, P. Strong convergence of the forward–backward splitting algorithms via linesearches in Hilbert spaces. *Appl. Anal.* **102** (2023), no. 5, 1394–1413.
[12] Kankam, K.; Pholasa, N.; Cholamjiak, P. Hybrid forward-backward algorithms using linesearch rule for minimization problem. *Thai J. Math.* **17** (2019), no. 3, 607–625.
[13] Kankam, K.; Pholasa, N.; Cholamjiak, P. On convergence and complexity of the modified forward-backward method involving new linesearches for convex minimization. *Math. Methods Appl. Sci.* **42** (2019), no. 5, 1352–1362.
[14] Khonchaliew, M.; Khamdam, K.; Petrot, N.; Plubtieng, S. Modified inertial subgradient extragradient with auxiliary parameters and parallel viscosity algorithm for minimization problem induced by bounded linear operator over common solution of fixed points of nonexpansive mappings and pseudomonotone equilibrium problems. *J. Math. Computer Sci.* **35** (2024), no. 2, 208–228.
[15] Lawanwadeekul S.; Bunma M. Analyzing the Performance of Ceramic Kiln by Using Thermal Image Technique for Reducing Energy Costs. *Key Eng. Mater.* **766** (2018), 7–12.
[16] Lawanwadeekul S.; Otsuru T.; Tomiku R.; Nishiguchi, H. Thermal-acoustic clay brick production with added charcoal for use in Thailand. *Constr. Build. Mater.* **255** (2020), 119376.
[17] Lawanwadeekul S.; Srisuwan A.; Phonphuak N.; and Chindaprasirt P. Enhancement of porosity and strength of clay brick fired at reduced temperature with the aid of corn cob and waste glass. *Constr. Build. Mater.* **369** (2023), 130547.
[18] Lawanwadeekul, S.; Chindaprasirt, P.; Phumiphan, A.; Srisuwan, A.; and Phonphuak, N. Transforming industrial waste by utilizing fly ash and bottom ash for sustainable clay bricks. *J. Mater. Cycles Waste Manag.* **2025** (2025), 1-15.
[19] Lee J.; Sanmugarasa K.; Blumenstein M.; Loo Y. C. Improving the reliability of a Bridge Management System (BMS) using an ANN-based Backward Prediction Model (BPM). *Autom. Constr.* **17** (2008), no. 6, 758–772.
[20] Matusik J.; Kłapyta Z.. Characterization of kaolinite intercalation compounds with benzyl alkylammonium chlorides using XRD, TGA/DTA and CHNS elemental analysis. *Appl. Clay Sci.* **83** (2013), 433–440.
[21] Moudafi, A.; Oliny, M. Convergence of a splitting inertial proximal method for monotone operators. *J. Comput. Appl. Math.* **155** (2003), no. 2, 447–454.
[22] Paama L., Pitkänen I., and Perämäki, P. Analysis of archaeological samples and local clays using ICP-AES, TG–DTG and FTIR techniques. *Talanta.* **51** (2000), no. 2, 349–357.
[23] Phonphuak N.; Thiansem, S. Effects of charcoal on physical and mechanical properties of fired test briquettes. *Sci. Asia.* **37** (2011), 120–124.
[24] Suantai, S.; Jailoka, P.; Hanjing, An accelerated viscosity forward-backward splitting algorithm with the linesearch process for convex minimization problems. *J. Inequal. Appl.* **2021** (2021), 42.
[25] Suantai, S.; Kankam, K.; Cholamjiak, P. A novel forward-backward algorithm for solving convex minimization problem in Hilbert spaces. *Mathematics.* **8** (2020), no. 1, 42.
[26] Suantai, S.; Kankam, K.; Cholamjiak, P. A projected forward-backward algorithm for constrained minimization with applications to image inpainting. *Mathematics.* **9** (2021), no. 8, 890.
[27] Suantai, S.; Noor, M. A.; Kankam, K.; Cholamjiak, P. Novel forward–backward algorithms for optimization and applications to compressive sensing and image inpainting. *Adv. Differ. Equ.* **2021** (2021), 265.
[28] Tikul N.; Srichandr P. Assessing the environmental impact of ceramic tile production in Thailand. *J. Ceram. Soc. Jpn.* **118** (2010), no. 1382, 887–894.
[29] Thai Industrial Standards Institute. *Thai Industrial Standard TIS 77–2545: Building brick*. Second edition. Ministry of Industry, Bangkok, Thailand 2002.
[30] Wolf A.; Rosendahl P. L.; Knaack, U. Additive manufacturing of clay and ceramic building components. *Autom. Constr.* **133** (2022), no. 1, 103956.
[31] Zhang Z.; Wong Y. C.; Arulrajah A.; Horpibulsuk, S. A review of studies on bricks using alternative materials and approaches. *Constr. Build. Mater.* **188** (2018), no. 11, 1101–1118.

[1] School of Science, University of Phayao, Phayao 56000, Thailand
Email address: watcharaporn.ch@up.ac.th
Email address: prasitch2008@yahoo.com

[2] FACULTY OF INDUSTRIAL TECHNOLOGY, LAMPANG RAJABHAT UNIVERSITY, LAMPANG 52100, THAILAND
Email address: b_siwat@g.lpru.ac.th

[3] ELEMENTARY EDUCATION PROGRAM, FACULTY OF EDUCATION, SUAN DUSIT UNIVERSITY LAMPANG CENTER, LAMPANG 52100, THAILAND
Email address: kunradazzz@gmail.com

[4] FACULTY OF SCIENCE, LAMPANG RAJABHAT UNIVERSITY, LAMPANG 52100, THAILAND
Email address: nipa.676@g.lpru.ac.th